

Fourier Domain Beamforming: The Path to Compressed Ultrasound Imaging

Tanya Chernyakova, *Student Member, IEEE*, Yonina C. Eldar, *Fellow, IEEE*

Abstract—Sonography techniques use multiple transducer elements for tissue visualization. Signals detected at each element are sampled prior to digital beamforming. The sampling rates required to perform high resolution digital beamforming are significantly higher than the Nyquist rate of the signal and result in considerable amount of data, that needs to be stored and processed. A recently developed technique, compressed beamforming, based on the finite rate of innovation model, compressed sensing (CS) and Xampling ideas, allows to reduce the number of samples needed to reconstruct an image comprised of strong reflectors. A drawback of this method is its inability to treat speckle, which is of significant importance in medical imaging. Here we build on previous work and extend it to a general concept of beamforming in frequency. This allows to exploit the low bandwidth of the ultrasound signal and bypass the oversampling dictated by digital implementation of beamforming in time. Using beamforming in frequency, the same image quality is obtained from far fewer samples. We next present a CS-technique that allows for further rate reduction, using only a portion of the beamformed signal's bandwidth. We demonstrate our methods on in vivo cardiac data and show that reductions up to 1/28 over standard beamforming rates are possible. Finally, we present an implementation on an ultrasound machine using sub-Nyquist sampling and processing. Our results prove that the concept of sub-Nyquist processing is feasible for medical ultrasound, leading to the potential of considerable reduction in future ultrasound machines size, power consumption and cost.

Index Terms—Array processing, beamforming, compressed sensing (CS), ultrasound, sub-Nyquist sampling.

I. INTRODUCTION

Diagnostic ultrasound has been used for decades to visualize body structures. Imaging is performed by transmitting a pulse along a narrow beam from an array of transducer elements. During its propagation echoes are scattered by acoustic impedance perturbations in the tissue, and detected by the array elements. The data, collected by the transducers, is sampled and digitally integrated in a way referred to as beamforming, which results in signal-to-noise ratio (SNR) enhancement and improvement of angular localization. Such a beamformed signal, referred to as beam, forms a line in the image.

According to the classic Shannon-Nyquist theorem [1], the minimal sampling rate at each transducer element should be at least twice the bandwidth of the detected signal in order to avoid aliasing. In practice, rates up to 4-10 times the central frequency of the transmitted pulse are required in order to eliminate artifacts caused by digital implementation of beamforming in time [2]. Taking into account the number of transducer elements and the number of lines in an image, the amount of sampled data that needs to be digitally processed

is enormous, motivating methods to reduce sampling and processing rates.

A possible approach to sampling rate reduction is introduced in [3]. Tur et al. consider the ultrasound signal detected by each receiver within the framework of finite rate of innovation (FRI) [4]. The detected signal is modeled as L replicas of a known pulse-shape, caused by scattering of the transmitted pulse from various reflectors, located along the transmitted beam. Such an FRI signal is fully described by $2L$ parameters, corresponding to the replica's unknown delays and amplitudes. Based on [4], the relationship between the signal's Fourier series coefficients and the unknown parameters is formulated in the form of a spectral analysis problem. The latter may be solved using array processing methods or compressed sensing (CS) techniques, given a subset of at least $2L$ Fourier series coefficients [5], [6]. The required Fourier coefficients can be computed from appropriate low-rate samples of the signal following ideas of [3], [7]–[10]. Recent work has developed a hardware prototype implementing the suggested sub-Nyquist system [11].

The above framework allows to sample the detected signals at a low-rate, assuming sufficiently high SNR. However, the final goal in low-rate ultrasound imaging is to recover a two-dimensional image, obtained by integrating the noisy data sampled at multiple transducer elements. In standard imaging the integration is achieved by the process of beamforming, which is performed digitally and, theoretically, requires high sampling rates. Hence, in order to benefit from the rate reduction achieved in [3], one needs to be able to incorporate beamforming into the low-rate sampling process.

A. Related Work: Compressed Beamforming

A solution to low-rate beamforming is proposed in [5], where Wagner et al. introduce the concept of compressed beamforming. They show that their approach, applied to an array of transducer elements, allows to reconstruct a two-dimensional ultrasound image depicting macroscopic perturbations in the tissue. To develop their method, the authors first prove that the beam obeys an FRI model, implying that it can be reconstructed from a small subset of its Fourier coefficients. However, this required subset cannot be obtained by the schemes proposed in [3] and [10], since the beam does not exist in the analog domain. It is constructed digitally after sampling the detected signals. This fundamental obstacle is resolved by transforming the beamforming operator into the compressed domain. Specifically, Wagner et al. show that the Fourier coefficients of the beam can be approximated by

a linear combination of Fourier coefficients of the detected signals. The latter are obtained from the low-rate samples of the detected signals, using the Xampling method, proposed in [3], [10] and [11].

Another innovation of [5] regards the approach to beam reconstruction from a subset of its frequency samples. Rather than use standard spectral analysis techniques, Wagner et al. view the reconstruction as a CS problem. They demonstrate that CS methodology is comparable to spectral analysis methods and even outperforms the latter when the noise is large. Combining compressed beamforming with CS techniques for signal recovery, they reconstruct two-dimensional ultrasound images, comprised of strong reflectors in the tissue. Significant rate reduction is achieved, while assuming that the number of replicas in the FRI model of the beam is small. Such an assumption is justified by the fact that only strong perturbations in the tissue are taken into account. Therefore, the proposed framework allows for robust detection of strong reflectors, but is unable to treat speckle, weak scattered echoes originating from microscopic perturbations in the tissue, which are of significant importance in medical imaging.

B. Contributions

In this paper we build on the results in [5] and show that compressed beamforming can be extended to a much more general concept of beamforming in frequency. This approach to beamforming is applicable to any signal, without the need to assume a structured model. When structure exists, beamforming in frequency may be combined with CS to yield further rate reduction.

The core of compressed beamforming is the relationship between the beam and the detected signals in the frequency domain, while the notion of “compressed” stems from the fact that the Fourier coefficients of the detected signals can be obtained from their low-rate samples. Here we show that this frequency domain relationship is general and holds irrespective of the FRI model. This leads to an approach of beamforming in frequency which is completely equivalent to beamforming in time. Beamforming in frequency is equivalent to a weighted averaging of the Fourier coefficients of the detected signals and can be performed efficiently by exploiting two facts. First, the frequency domain beamforming operator is defined by the geometry of the transducer array and does not depend on the detected signals. Hence, the required weights can be computed off-line and used as a look-up-table during the imaging cycle. In addition, we show numerically, that these weights are characterized by a rapid decay, implying that the Fourier coefficients of the beam can be computed using a small number of Fourier coefficients of the detected signals.

Next, we show that beamforming in frequency domain allows to bypass the oversampling dictated by digital implementation of beamforming in time. Since the beam is obtained directly in frequency, we need to compute its Fourier coefficients only within its effective bandwidth. We demonstrate that this can be achieved using generalized samples of the detected signals, obtained at their Nyquist rate. To avoid confusion, by Nyquist rate we mean the signals effective bandpass

bandwidth, which is typically much lower than its highest frequency since the detected pulse is normally modulated onto a carrier and only occupies a portion of the entire bandwidth. Using in vivo cardiac data, we illustrate that beamforming in frequency allows to preserve image integrity with 4-10 fold reduction in the number of samples used for its reconstruction.

Further reduction in sampling rate is obtained, similarly to [5], when only a portion of the beam’s bandwidth is used. In this case beamforming in frequency is equivalent to compressed beamforming. Detected signals are sampled at sub-Nyquist rates, leading to up to 28 fold reduction in sampling rate. Our contribution in this scenario regards the reconstruction method used to recover the beam from its partial frequency data. To recover the unknown parameters, corresponding to the FRI model of the beam, Wagner et al. assume that the parameter vector is sparse. The parameters are then obtained as a solution of an l_0 optimization problem. Sparsity holds when only strong reflectors are taken into account, while the speckle is treated as noise. To capture the speckle, we assume that the parameter vector is compressible and recast the recovery as an l_1 optimization problem. We show that these small changes in the model and the CS reconstruction technique allow to capture and recover the speckle, leading to significant improvement in image quality.

Finally, we introduce an implementation of beamforming in frequency and sub-Nyquist processing on a stand alone ultrasound machine and show that our proposed processing is feasible in practice using real hardware. Low-rate processing is performed on the data obtained in real-time by scanning a heart with a 64-element probe. Our approach allows for significant rate reduction with respect to the lowest processing rates that are achievable today, which can potentially impact system size, power consumption and cost.

The rest of the paper is organized as follows: in Section II, we review beamforming in time and discuss the sampling rates required for its digital implementation. Following the steps in [5], we describe the principles of frequency domain beamforming in Section III, and show that it is equivalent to standard time domain processing. In Section IV we show that beamforming in frequency allows for rate reduction even without exploiting the FRI model and can be performed at the Nyquist rate of the signal. CS recovery from partial frequency data, implying sampling and processing at sub-Nyquist rates, is discussed in Section V. Comparison between the performance of the proposed method with the results obtained in [5] together with an implementation of beamforming in frequency and sub-Nyquist processing on a stand alone ultrasound machine are presented in Section VI.

II. CONVENTIONAL PROCESSING IN ULTRASOUND IMAGING

Most modern imaging systems use multiple transducer elements to transmit and receive acoustic pulses. This allows to perform beamforming during both transmission and reception. Beamforming is a common signal-processing technique [12] that enables spatial selectivity of signal transmission or

reception and is applied in various fields, including wireless communication, speech processing, radar and sonar. In ultrasound imaging beamforming is used for steering the beam in a desired direction and focusing it in the region of interest in order to detect tissue structures.

During transmission beamforming is achieved by delaying the transmission time of each transducer element, which allows to transmit energy along a narrow beam. Beamforming upon reception is much more challenging. Here dynamically changing delays are applied on the signals detected at each one of the transducer elements prior to averaging. Time-varying delays allow dynamic shift of the reception beam's focal point, optimizing angular resolution. Averaging of the delayed signals in turn enhances the SNR of the resulting beamformed signal, which is used to form a line in an image. From here on, the term beamforming will refer to beamforming on reception, which is the focus of this work.

A. Beamforming in Time

We begin with a detailed description of the beamforming process which takes place in a typical B-mode imaging cycle. Our presentation is based mainly on [13] and [5]. We will then show, in Section III, how the same process can be performed in frequency, paving the way to substantial rate reduction.

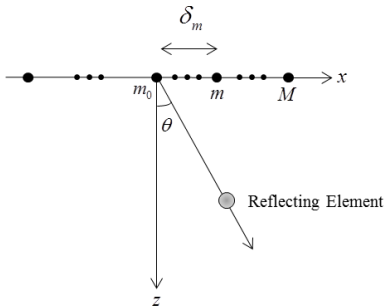


Fig. 1. M receivers aligned along the x axis. An acoustic pulse is transmitted in a direction θ . The echoes scattered from perturbation in the radiated tissue are received by the array elements.

In the transmit path, a pulse is generated and transmitted by the array of transducer elements. The pulse transmitted by each element is timed and scaled, so that the superposition of all transmitted pulses creates a directional beam propagating at a certain angle. By subsequently transmitting at different angles, a whole sector is radiated. The real time computational complexity in the transmit path is negligible since transmit parameters per angle are calculated off-line and saved in tables.

Consider an array comprised of M transceiver elements aligned along the x axis, as illustrated in Fig. 1. The reference element m_0 is set at the origin and the distance to the m th element is denoted by δ_m . The image cycle begins at $t = 0$, when the array transmits an energy pulse in the direction θ . The pulse propagates through the tissue at speed c , and at time $t \geq 0$ its coordinates are $(x, z) = (ct \sin \theta, ct \cos \theta)$. A potential point reflector located at this position scatters the energy, such that the echo is detected by all array elements at a time depending on their locations. Denote by $\varphi_m(t; \theta)$ the

signal detected by the m th element and by $\hat{\tau}_m(t; \theta)$ the time of detection. It is readily seen that:

$$\hat{\tau}_m(t; \theta) = t + \frac{d_m(t; \theta)}{c}, \quad (1)$$

where $d_m(t; \theta) = \sqrt{(ct \cos \theta)^2 + (\delta_m - ct \sin \theta)^2}$ is the distance traveled by the reflection. Beamforming involves averaging the signals detected by multiple receivers while compensating the differences in detection time. In that way we obtain a signal containing the intensity of the energy reflected from each point along the central transmission axis θ .

Using (1), the detection time at m_0 is $\hat{\tau}_{m_0}(t; \theta) = 2t$ since $\delta_{m_0} = 0$. Applying an appropriate delay to $\varphi_m(t; \theta)$, such that the resulting signal $\hat{\varphi}_m(t; \theta)$ satisfies $\hat{\varphi}_m(2t; \theta) = \varphi_m(\hat{\tau}_m(t; \theta))$, we can align the reflection detected by the m -th receiver with the one detected at m_0 . Denoting $\tau_m(t; \theta) = \hat{\tau}_m(t/2; \theta)$ and using (1), the following aligned signal is obtained:

$$\begin{aligned} \hat{\varphi}_m(t; \theta) &= \varphi_m(\tau_m(t; \theta); \theta), \\ \tau_m(t; \theta) &= \frac{1}{2} \left(t + \sqrt{t^2 - 4(\delta_m/c)t \sin \theta + 4(\delta_m/c)^2} \right). \end{aligned} \quad (2)$$

The beamformed signal may now be derived by averaging the aligned signals:

$$\Phi(t; \theta) = \frac{1}{M} \sum_{m=1}^M \hat{\varphi}_m(t; \theta). \quad (3)$$

Such a beam is optimally focused at each depth and hence exhibits improved angular localization and enhanced SNR.

Although defined over continuous time, ultrasound imaging systems perform the beamforming process in (2)-(3) in the digital domain: analog signals $\varphi_m(t; \theta)$ are amplified and sampled by an Analog to Digital Converter (ADC), preceded by an anti-aliasing filter. We next discuss sampling and processing rates required to perform (3).

B. Rate Requirements

Digital implementation of beamforming requires sampling the signals detected at the transducer elements and transmitting the samples to the processing unit. The Nyquist rate, required to avoid aliasing, is insufficient for digital implementation of beamforming due to the high delay resolution needed. Indeed, in order to apply the delay defined in (2) digitally, detected signals need to be sampled on a sufficiently dense grid. Typically, the sampling interval is on the order of nanoseconds. Therefore, required sampling rates are significantly higher than the Nyquist rate of the signal and can be as high as hundreds of MHz [14].

Due to the impracticality of this requirement, ultrasound data is sampled at lower rates, typically, on the order of tens of MHz. Fine delay resolution is obtained by subsequent digital interpolation. Interpolation beamforming allows to reduce the sampling rate at the cost of additional computational load required to implement the digital interpolation which effectively increases the rate in the digital domain. The processing, or more precisely, beamforming rate, remains unchanged as it is performed at the high digital rate.

Another common way to improve delay accuracy while reducing both sampling and beamforming rate is phase-rotation-based beamforming (PRBF) [2]. In this approach coarse delays, defined by the sampling rate, are followed by a vernier control, implemented by a digital phase shift, adjusted for the central frequency. The phase shifter approximation to a time delay is exact only at the central frequency, leading to loss in array gain and rise in the sidelobe level. The analysis in [2] shows that the degradation of beam quality can be avoided, provided that the sampling rate is 4-10 times the transducer central frequency. This rule of thumb stems from the assumption that typically the transducer central frequency is approximately twice the radio frequency (RF) bandwidth. RF bandwidth is defined as the distance from the central to the highest frequency and, hence, is half the bandpass bandwidth. This leads to the conclusion that the sampling rate should be about 4-10 times the bandpass bandwidth, since, according to the analysis in [2], loss in array gain and rise in the sidelobe level are dictated by the ratio between the bandwidth of the signal to the sampling rate. In the sequel, following [2], we denote the rate required to avoid artifacts in digital implementation of beamforming, as the beamforming rate f_s .

As imaging systems evolve, the amount of elements participating in the imaging cycle continues to grow significantly. Consequently large amounts of data need to be transmitted from the system front-end and digitally processed in real time. Increasing transmission and processing pose an engineering challenge on digital signal processing (DSP) hardware and motivate reducing the amounts of data as close as possible to the system front-end.

To conclude this section we evaluate the sampling rates and the number of samples needed to be taken at each transducer element according to each one of the methods, described above. Our evaluation is based on the imaging setup typically used in cardiac imaging. We assume a breadboard ultrasonic scanner of 64 acquisition channels. The radiated depth $r = 16$ cm and speed of sound $c = 1540$ m/sec yield a signal of duration $T = 2r/c \simeq 210$ μ sec. The acquired signal is characterized by a narrow bandpass bandwidth of 2 MHz, centered at the carrier frequency $f_0 \approx 3.4$ MHz. In order to perform plain delay-and-sum beamforming with 5 nsec delay resolution, detected signals should be sampled at the rate of 200 MHz. Implementation of interpolation beamforming, used in many imaging systems, allows to reduce the sampling rate to 50 MHz, while the required beamforming rate is obtained through interpolation in the digital domain. Hence, each channel yields 42000 real valued samples, participating in beamforming. Rates required by PRBF in this setup, vary from 8 to 20 MHz, leading to 1680-4200 real valued samples, obtained at each transducer element.

Evidently, processing in the time domain imposes high sampling rate and considerable burden on the beamforming block. We next show that the number of samples can be reduced significantly by exploiting ideas of sub-Nyquist sampling, beamforming in frequency and CS-based signal reconstruction.

III. BEAMFORMING IN FREQUENCY

We now show that beamforming can be performed equivalently in the frequency domain, paving the way to substantial reduction in the number of samples needed to obtain the same image quality. We extend the notion of compressed beamforming, introduced in [5], to beamforming in frequency and show that a linear combination of the discrete Fourier transform (DFT) coefficients of the individual signals, sampled at the beamforming rate f_s , yields the DFT coefficients of the beamformed signal, sampled at the same rate. This relationship is true irrespective of the signal structure.

A. Implementation and Properties

We follow the steps in [5] and start from the computation of the Fourier series coefficients of the beam $\Phi(t; \theta)$. As shown in [5], the support of the beam $\Phi(t; \theta)$ is limited to $[0, T_B(\theta))$, where $T_B(\theta) < T$ and T is defined by the transmitted pulse penetration depth. The value of $T_B(\theta)$ is given by [5]

$$T_B(\theta) = \min_{1 \leq m \leq M} \tau_m^{-1}(T; \theta), \quad (4)$$

where $\tau_m(t; \theta)$ is defined in (2). Denote the Fourier series coefficients of $\Phi(t; \theta)$ with respect to the interval $[0, T)$ by

$$c_k^s = \frac{1}{T} \int_0^T I_{[0, T_B(\theta))}(t) \Phi(t; \theta) e^{-i \frac{2\pi}{T} kt} dt, \quad (5)$$

where $I_{[a, b)}$ is the indicator function equal to 1 when $a \leq t < b$ and 0 otherwise. Plugging (3) into (5), and after some algebraic manipulation, it is shown in [5] that

$$c_k^s = \frac{1}{M} \sum_{m=1}^M c_{k, m}^s, \quad (6)$$

where $c_{k, m}^s$ are defined as follows:

$$c_{k, m}^s = \frac{1}{T} \int_0^T g_{k, m}(t; \theta) \varphi_m(t; \theta) dt, \quad (7)$$

with

$$\begin{aligned} g_{k, m}(t; \theta) &= q_{k, m}(t; \theta) e^{-i \frac{2\pi}{T} kt}, \\ q_{k, m}(t; \theta) &= I_{[|\gamma_m|, \tau_m(T; \theta))}(t) \left(1 + \frac{\gamma_m^2 \cos^2 \theta}{(t - \gamma_m \sin \theta)^2} \right) \times \\ &\quad \exp \left\{ i \frac{2\pi}{T} k \frac{\gamma_m - t \sin \theta}{t - \gamma_m \sin \theta} \gamma_m \right\}, \end{aligned} \quad (8)$$

and $\gamma_m = \delta_m/c$.

The next step is to replace $\varphi_m(t)$ by its Fourier series coefficients. Denoting the n th Fourier coefficient by $\varphi_m^s[n]$ and using (8) we can rewrite (7) as

$$c_{k, m}^s = \sum_n \varphi_m^s[k - n] Q_{k, m; \theta}[n], \quad (9)$$

where $Q_{k, m; \theta}[n]$ are the Fourier coefficients of the distortion function $q_{k, m}(t; \theta)$ with respect to $[0, T)$. According to Proposition 1 in [5], $c_{k, m}^s$ can be approximated sufficiently well when we replace the infinite summation in (9) by a finite sum:

$$c_{k, m}^s \simeq \sum_{n \in \nu(k)} \varphi_m^s[k - n] Q_{k, m; \theta}[n]. \quad (10)$$

The set $\nu(k)$ depends on the decay properties of $\{Q_{k,m;\theta}[n]\}$.

We now take a closer look at the properties of the Fourier coefficients of $q_{k,m}(t; \theta)$, defined in (8). Numerical studies show that most of the energy of the set $\{Q_{k,m;\theta}[n]\}$ is concentrated around the direct current (DC) component. This behavior is typical to any choice of k , m or θ . An example for $k = 100$, $m = 14$ and $\theta = 0.421$ [rad] is shown in Fig. 2. This allows us to rewrite (10) as

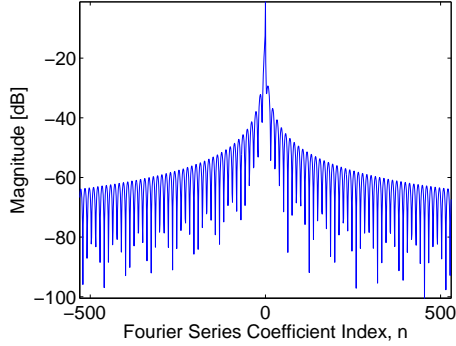


Fig. 2. Fourier coefficients $\{Q_{k,m;\theta}[n]\}$ of $q_{k,m}(t; \theta)$ are characterized by a rapid decay, where most of the energy is concentrated around the DC component. Here $k = 100$, $m = 14$ and $\theta = 0.421$ [rad].

$$c_{k,m}^s \simeq \sum_{n=-N_1}^{N_2} \varphi_m^s[k-n]Q_{k,m;\theta}[n]. \quad (11)$$

The choice of N_1 and N_2 controls the approximation quality. Numerical studies show that 20 most significant elements of $\{Q_{k,m;\theta}[n]\}$ contain, on average, more than 95% of the entire energy irrespective of the choice of k , m or θ . Beamforming in frequency therefore is performed using 20 most significant elements in $\{Q_{k,m;\theta}[n]\}$ throughout our work.

Denote by β , $|\beta| = B$, the set of Fourier coefficients of the detected signal that correspond to its bandwidth, namely, the values of k for which $\varphi_m^s[k]$ is nonzero (or larger than a threshold). Note that (11) implies, that the bandwidth of the beam, β_{BF} , will contain at most $(B + N_1 + N_2)$ nonzero frequency components. To compute the elements in β_{BF} all we need is the set β for each one of the detected signals. In a typical imaging setup B is of order of hundreds of coefficients, while N_1 and N_2 , defined by the decaying properties of $\{Q_{k,m;\theta}[n]\}$, are no larger than 10. This implies that $B \gg N_i, i \in \{1, 2\}$, so $B + N_1 + N_2 \approx B$. Hence, the bandwidth of the beam is approximately equal to the bandwidth of the detected signals. In addition, it follows from (11) that in order to calculate an arbitrary subset $\mu \subset \beta_{BF}$ of size M of Fourier coefficients of the beam, we need to know at most $(M + N_1 + N_2)$ Fourier coefficients of each one of the detected signals $\varphi_m(t)$. These properties of frequency domain beamforming will be used in order to reduce sampling rates.

Equations (6) and (11) provide a relationship between the Fourier series coefficients of the beam and the individual signals. We next derive a corresponding relationship between the DFT coefficients of the above signals, sampled at the beamforming rate f_s . Denote by $N = \lfloor T \cdot f_s \rfloor$ the resulting number of samples. Since f_s is higher than the Nyquist rate of

the detected signals, the relation between the DFT of length N and the Fourier series coefficients of $\varphi_m(t)$ is given by [15]:

$$\varphi_m^s[n] = \frac{1}{N} \begin{cases} \varphi_m[n], & 0 \leq n \leq P \\ \varphi_m[N+n], & -P \leq n < 0 \\ 0, & \text{otherwise,} \end{cases} \quad (12)$$

where $\varphi_m[n]$ denote the DFT coefficients and P denotes the index of the Fourier transform coefficient, corresponding to the highest frequency component.

We can use (12) to substitute Fourier series coefficients $\varphi_m^s[n]$ of $\varphi_m(t)$ in (11) by DFT coefficients $\varphi_m[n]$ of its sampled version. Plugging the result into (6), we obtain a relationship between Fourier series coefficients of the beam and DFT coefficients of the sampled detected signals:

$$c_k^s \simeq \frac{1}{MN} \sum_{m=1}^M \sum_{n=-N_1}^{k-\tilde{n}} \varphi_m[k-n]Q_{k,m;\theta}[n] \quad (13) \\ + \sum_{n=k-\tilde{n}+1}^{N_2} \varphi_m[k-n+N]Q_{k,m;\theta}[n]$$

for an appropriate choice of \tilde{n} . Since f_s is higher than the Nyquist rate of the beam as well, the DFT coefficients c_k of its sampled version are given by an equation similar to (12):

$$c_k = N \begin{cases} c_k^s, & 0 \leq k \leq P \\ c_{k-N}^s, & N-P \leq k < N \\ 0, & \text{otherwise.} \end{cases} \quad (14)$$

Equations (13) and (14) provide the desired relationship between the DFT coefficients of the beam and the DFT coefficients of the detected signals. Note that this relationship, obtained by a periodic shift and scaling of (11), retains the important properties of the latter.

Applying an IDFT on $\{c_k\}_{k=0}^{N-1}$ results in the beamformed signal in time. We can now proceed to standard image generation steps which include log-compression and interpolation.

B. Simulations and Validation

To demonstrate the equivalence of beamforming in time and frequency, we applied both methods on in vivo cardiac data yielding the images shown in Fig. 3. The imaging setup is that described in Section II-B with $f_s = 16$ MHz. As can be readily seen, the images look identical.

Quantitative validation of the proposed method was performed with respect to both one-dimensional beamformed signals and the resulting two-dimensional image. To compare the one-dimensional signals, we calculated the normalized root-mean-square error (NRMSE) between the signals obtained by beamforming in frequency and those obtained by standard beamforming in time. Both class of signals were compared after envelope detection, performed by a Hilbert transform in order to remove the carrier. Denote by $\Phi[n; \theta_j]$ the signal obtained by standard beamforming in direction θ_j , $j = 1, \dots, J$, and let $\hat{\Phi}[n; \theta_j]$ denote the signal obtained by beamforming in frequency. The Hilbert transform is denoted by $H(\cdot)$. For the

set of $J = 120$ image lines, we define NRMSE as:

$$NRMSE = \frac{1}{J} \sqrt{\frac{\sum_{n=1}^N \left(H(\Phi[n; \theta_j]) - H(\hat{\Phi}[n; \theta_j]) \right)^2}{H(\Phi[n; \theta_j])_{max} - H(\Phi[n; \theta_j])_{min}}}, \quad (15)$$

where $H(\Phi[n; \theta_j])_{max}$ and $H(\Phi[n; \theta_j])_{min}$ denote the maximal and minimal values of the envelope of the beamformed signal in time.

Comparison of the resulting images was performed by calculating the structural similarity (SSIM) index [16], commonly used for measuring similarity between two images. The first line of Table I summarizes the resulting values. These values verify that both 1D signals and the resulting image are extremely similar.

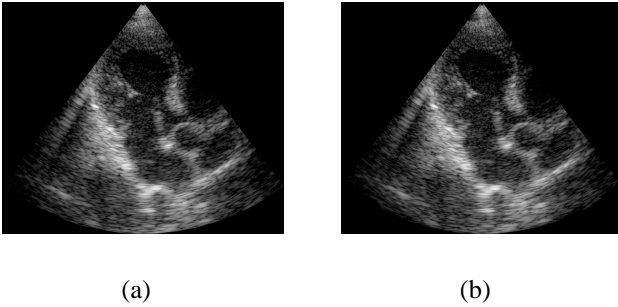


Fig. 3. Cardiac images constructed with different beamforming techniques. (a) Time domain beamforming. (b) Frequency domain beamforming.

IV. RATE REDUCTION BY BEAMFORMING IN FREQUENCY

In the previous section we showed the equivalence of beamforming in time and frequency. We next demonstrate that beamforming in frequency allows to reduce the required number of samples of the individual signals. Reduction can be achieved in two different ways. First, we exploit the low effective bandwidth of ultrasound signals and bypass oversampling, dictated by digital implementation of beamforming in time. This allows to perform processing at the Nyquist rate, defined with respect to the effective bandwidth of the signal, which is impossible when beamforming is performed in time. As a second step, we show that further rate reduction is possible, when we take into account the FRI structure of the beamformed signal and use CS techniques for recovery.

In this section we address rate reduction, obtained by translation of the beamforming operator into the frequency domain. At this stage the structure of the beamformed signal is not taken into account.

A. Exploiting Frequency Domain Relationship

To reduce the rate, we exploit the relationship between the beam and the detected signals in the frequency domain given by (11). In Section III-A, we showed that the bandwidth of the beam, β_{BM} , contains approximately B nonzero frequency components, where B is the effective bandwidth of the detected signals. In order to compute β_{BM} we need a set β of nonzero frequency components of each one of the detected

signals. This allows to exploit the low effective bandwidth of the detected signals and calculate only their nonzero DFT coefficients. The ratio between the cardinality of the set β and the overall number of samples N , required by standard beamforming rate f_s , is dictated by the oversampling factor. As mentioned in Section II-B, we define f_s as 4-10 times the bandpass bandwidth of the detected signal, leading to $B/N = 1/4-1/10$. Assume that it is possible to obtain the required set β using B low-rate samples of the detected signal. In this case the ratio between N and B implies potential 4-10 fold reduction in the required sampling rate.

B. Reduced Rate Sampling

We now address the following question: how do we obtain the required set β , corresponding to the effective bandpass bandwidth, using B low-rate samples of each one of the detected signals?

Note that sampling is performed in time, while our goal is to extract B DFT coefficients. To this end, similarly to [5], we can use the Xampling mechanism proposed in [3]. A hardware Xampling prototype implemented by Baransky et al. in [11] is seen in Fig. 4.



Fig. 4. A Xampling-based hardware prototype for sub-Nyquist sampling. The prototype computes low-rate samples of the input from which the set β of DFT coefficients can be computed on the outputs.

The Xampling scheme allows to obtain B coefficients from B point-wise samples of the detected signal filtered with an appropriate kernel $s^*(-t)$, designed according to the transmitted pulse-shape and the set β . The required DFT coefficients are equal to the DFT of the outputs, therefore, the number of samples taken at each individual element is equal to the number of DFT coefficients that we want to compute. Hence, when we compute all nonzero DFT coefficients of the detected signal, 4-10 fold reduction in sampling rate is achieved without compromising image quality.

Having obtained the set β of each one of the detected signals, we calculate the elements of β_{BF} by low-rate frequency domain beamforming. Finally, we reconstruct the beamformed signal in time by performing an IDFT. Note that it is possible to pad the elements of β_{BF} with an appropriate number of zeros to improve time resolution. In our experiments, in order to compare the proposed method with standard processing, we padded β_{BF} with $N - B$ zeros, leading to the same sampling grid, used for high-rate beamforming in time.

Images obtained by the proposed method, using 416 real-valued samples per image line to perform beamforming in frequency, and by standard beamforming, using 3360 real-valued samples to perform beamforming in time, are shown in Fig. 5. Corresponding values of NRMSE and SSIM are reported in the

second line of Table I. These values validate close similarity between the two methods. However, in this case NRMSE is slightly higher, while SSIM is lower, compared to the values obtained in Section III-B. Note that these values depict similarity between the signals. Differences can therefore be explained by the following practical aspect. When we obtain the set of all nonzero DFT coefficients of the beamformed signal, β_{BF} , all the signal energy is captured in the frequency domain. However, the signal obtained by beamforming in time, contains noise, which occupies the entire spectrum. When only the DFT coefficients within the bandwidth are computed in the frequency domain, the noise outside the bandwidth is effectively filtered out. In the signal obtained by standard beamforming, the noise is retained, reducing the similarity between the two signals.

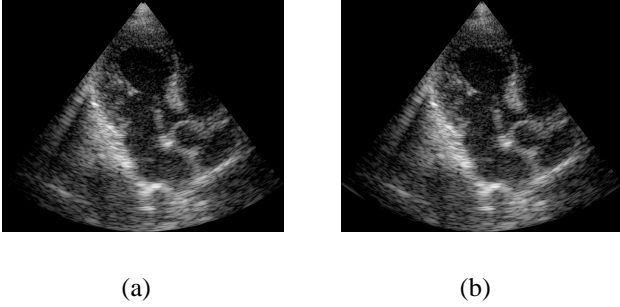


Fig. 5. Cardiac images constructed with different beamforming techniques. (a) Time domain beamforming. (b) Frequency domain beamforming, obtained with 8 fold reduction in sampling rate.

The entire scheme, performing low-rate sampling and frequency domain beamforming, is depicted in Fig. 6. Signals $\{\varphi_m(t)\}_{m=1}^M$, detected at each transducer element, are filtered with an appropriate analog kernel $s^*(-t)$ and sampled at a low-rate, defined by the effective bandwidth of the transmitted pulse. Such a rate corresponds to the Nyquist rate of the baseband transmitted pulse. DFT coefficients of the detected signals are computed and beamforming is performed directly in frequency at a low-rate. This framework allows to bypass oversampling dictated by digital implementation of beamforming in time and to significantly reduce (up to 10-fold) the resulting sampling rate.

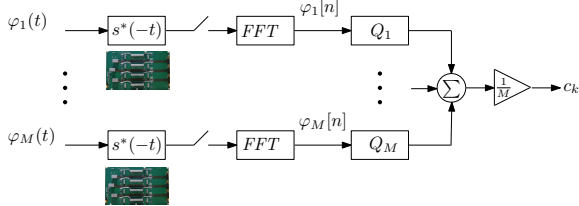


Fig. 6. Fourier domain beamforming scheme. The block Q_i represents averaging the DFT coefficients of the detected signals with weights $\{Q_{k,i;\theta}[n]\}$ according to (13) and (14).

V. FURTHER REDUCTION VIA COMPRESSED SENSING

We have shown that it is possible to reconstruct a beamformed signal perfectly from a set β_{BF} of its nonzero DFT

TABLE I
QUANTITATIVE VALIDATION OF BEAMFORMING IN FREQUENCY WITH
RESPECT TO BEAMFORMING IN TIME

Method	NRMSE	SSIM
Beamforming in frequency	0.0349	0.9684
Beamforming in frequency, reduced rate sampling	0.0368	0.9603

coefficients. In this section we consider further reduction in sampling rate by taking only a subset $\mu \subset \beta_{BF}$, $|\mu| = M < B_{BF} = |\beta_{BF}|$, of nonzero DFT coefficients. In this case, as shown in Section III-A, $(M + N_1 + N_2)$ frequency components of each one of the detected signals are required, leading to only $(M + N_1 + N_2)$ samples in each channel. The challenge now is to reconstruct a beamformed signal from such partial frequency data.

To this end we aim to use CS techniques, while exploiting the FRI structure of the beamformed signal. To formulate the recovery as a CS problem, we begin with a parametric representation of the beam.

A. Parametric representation

According to [5], a beamformed signal obeys an FRI model, namely, it can be modeled as a sum of replicas of the known transmitted pulse, $h(t)$, with unknown amplitudes and delays:

$$\Phi(t; \theta) \simeq \sum_{l=1}^L \tilde{b}_l h(t - t_l), \quad (16)$$

where L is the number of scattering elements in direction θ , $\{\tilde{b}_l\}_{l=1}^L$ are the unknown amplitudes of the reflections and $\{t_l\}_{l=1}^L$ denote the times at which the reflection from the l th element arrived at the reference receiver m_0 . Since the transmitted pulse is known, such a signal is completely defined by $2L$ unknown parameters, the amplitudes and the delays.

We can rewrite this model accordingly by sampling both sides of (16) at the beamforming rate f_s and quantizing the unknown delays $\{t_l\}_{l=1}^L$ with quantization step $1/f_s$, such that $t_l = q_l/f_s$, $q_l \in \mathbb{Z}$ and $N = \lfloor T \cdot f_s \rfloor$:

$$\Phi[n; \theta] \simeq \sum_{l=1}^L \tilde{b}_l h[n - q_l] = \sum_{l=0}^{N-1} b_l h[n - l], \quad (17)$$

where

$$b_l = \begin{cases} \tilde{b}_l, & \text{if } l = q_l \\ 0, & \text{otherwise.} \end{cases} \quad (18)$$

Calculating the DFT of both sides of (17) leads to the following expression for the DFT coefficients c_k :

$$c_k = \sum_{n=0}^{N-1} \Phi[n; \theta] e^{-i \frac{2\pi}{N} kn} = h_k \sum_{l=0}^{N-1} b_l e^{-i \frac{2\pi}{N} kl}, \quad (19)$$

where h_k is the DFT coefficient of $h[n]$, the transmitted pulse sampled at rate f_s . We conclude that recovering $\Phi[n; \theta]$ is equivalent to determining b_l , $0 \leq l \leq N - 1$ in (19).

We now recast the problem in vector-matrix notation. Defining an M -length measurement vector \mathbf{c} with k th entry $c_k, k \in \mu$, we can rewrite (19) as follows:

$$\mathbf{c} = \mathbf{H}\mathbf{D}\mathbf{b} = \mathbf{A}\mathbf{b}, \quad (20)$$

where \mathbf{H} is an $M \times M$ diagonal matrix with h_k as its k th entry, \mathbf{D} is an $M \times N$ matrix formed by taking the set μ of rows from an $N \times N$ DFT matrix, and \mathbf{b} is a length- N vector with l th entry b_l .

Our goal is to determine \mathbf{b} from \mathbf{c} . We next discuss and compare possible recovery approaches.

B. Prior Work

As mentioned in Section V-A, the signal of interest is completely defined by L the unknown delays and amplitudes. Hence, a possible approach is to extract those values from the available set μ of DFT coefficients. To this end, we can view (20) as a complex sinusoid problem. For $M \geq 2L$ it can be solved using standard spectral analysis methods such as matrix pencil [17] or annihilating filter [18]. Rate reduction is achieved when $2L \ll N$, where N is the number of samples dictated by the standard beamforming rate.

In the presence of moderate to high noise levels, the unknown parameters can be extracted more efficiently using a CS approach, as was shown in [5]. Note that (20) is an underdetermined system of linear equations which has infinitely many solutions, since \mathbf{A} is an $M \times N$ matrix with $M \ll N$. The solution set can be narrowed down to a single value by exploiting the structure of the unknown vector \mathbf{b} . In the CS framework it is assumed that the vector of interest is reasonably sparse, whether in the standard coordinate basis or with respect to some other basis.

The regularization introduced in [5], relies on the assumption that the coefficient vector \mathbf{b} is L -sparse. The formulation in (20) then has a form of a classic CS problem, where the goal is to reconstruct an N -dimensional L -sparse vector \mathbf{b} from its projection onto K orthogonal rows captured by the measurement matrix \mathbf{A} . This problem can be solved using numerous CS techniques, when \mathbf{A} satisfies well-known properties such as restricted isometry (RIP) or coherence [6].

In our case, \mathbf{A} , defined in (20), is formed by taking K scaled rows from an $N \times N$ DFT matrix. It can be shown that by choosing $K \geq CL(\log N)^4$ rows uniformly at random for some positive constant C , the measurement matrix \mathbf{A} obeys the RIP with high probability [19]. In order for this approach to be beneficial it is important to assume that $L \ll N$. Since random frequency sampling is not practical from a hardware perspective, it is possible instead to sample a number of frequency bands, distributed randomly throughout the spectrum [11]. This approach is implemented in the board of Fig. 4.

A typical beamformed ultrasound signal is comprised of a relatively small number of strong reflections, corresponding to strong perturbations in the tissue, and many weaker scattered echoes, originated from microscopic changes in acoustic impedance of the tissue. The framework proposed in [5] aims to recover only strong reflectors in the tissue and treat weak

echoes as noise. Hence, the vector of interest \mathbf{b} is indeed L -sparse with $L \ll N$. To recover \mathbf{b} , Wagner et al. consider the following optimization problem:

$$\min_{\mathbf{b}} \|\mathbf{b}\|_0 \quad \text{subject to} \quad \|\mathbf{A}\mathbf{b} - \mathbf{c}\|_2 \leq \varepsilon, \quad (21)$$

where ε is an appropriate noise level, and approximate its solution using orthogonal matching pursuit (OMP) [20].

A significant drawback of this method is its inability to restore weak reflectors. In the context of this approach they are treated as noise and are disregarded by the signal model. As a result, the speckle - granular pattern that can be seen in Fig. 3 - is lost. This severely degrades the value of the resulting images since information carried by speckle is of major importance in many medical imaging modalities. For example, in cardiac imaging, speckle tracking tools allow to analyze the motion of heart tissues and to track effectively myocardial deformations [21], [22].

C. Alternative Approach

Fortunately, with a small conceptual change of model, we can restore the entire signal, namely, recover both strong reflectors and weak scattered echoes.

As mentioned above, a beamformed ultrasound signal is comprised of a relatively small number of strong reflections and many scattered echoes, that are on average two orders of magnitude weaker. It is, therefore, natural to assume that the coefficient vector \mathbf{b} , defined in (20), is compressible or approximately sparse, but not exactly sparse. This property of \mathbf{b} can be captured by using the l_1 norm, leading to the optimization problem:

$$\min_{\mathbf{b}} \|\mathbf{b}\|_1 \quad \text{subject to} \quad \|\mathbf{A}\mathbf{b} - \mathbf{c}\|_2 \leq \varepsilon. \quad (22)$$

Problem (22) can be solved using second-order methods such as interior point methods [23], [24] or first-order methods, based on iterative shrinkage ideas [25], [26].

We emphasize that although it is common to view (22) as a convex relaxation of (21), in our case such a substitution is crucial. It allows to capture the structure of the signal and to boost the performance of sub-Nyquist processing, as will be shown next, through several examples.

VI. SIMULATIONS AND RESULTS

In this section we examine the performance of low-rate frequency-domain beamforming using l_1 optimization and compare it to the previously proposed l_0 optimization based method. This is done by applying both methods to stored RF data, acquired from a healthy volunteer. We then integrate our method into a stand alone ultrasound machine and show that such processing is feasible in practice using real hardware.

A. Simulations on In Vivo Cardiac Data

To demonstrate low-rate beamforming in frequency and evaluate the impact of rate reduction on image quality, we applied our method on in vivo cardiac data. The data acquisition setup is described in Section II-B with $f_s = 16$ MHz, leading to 3360 real valued samples. To perform beamforming in

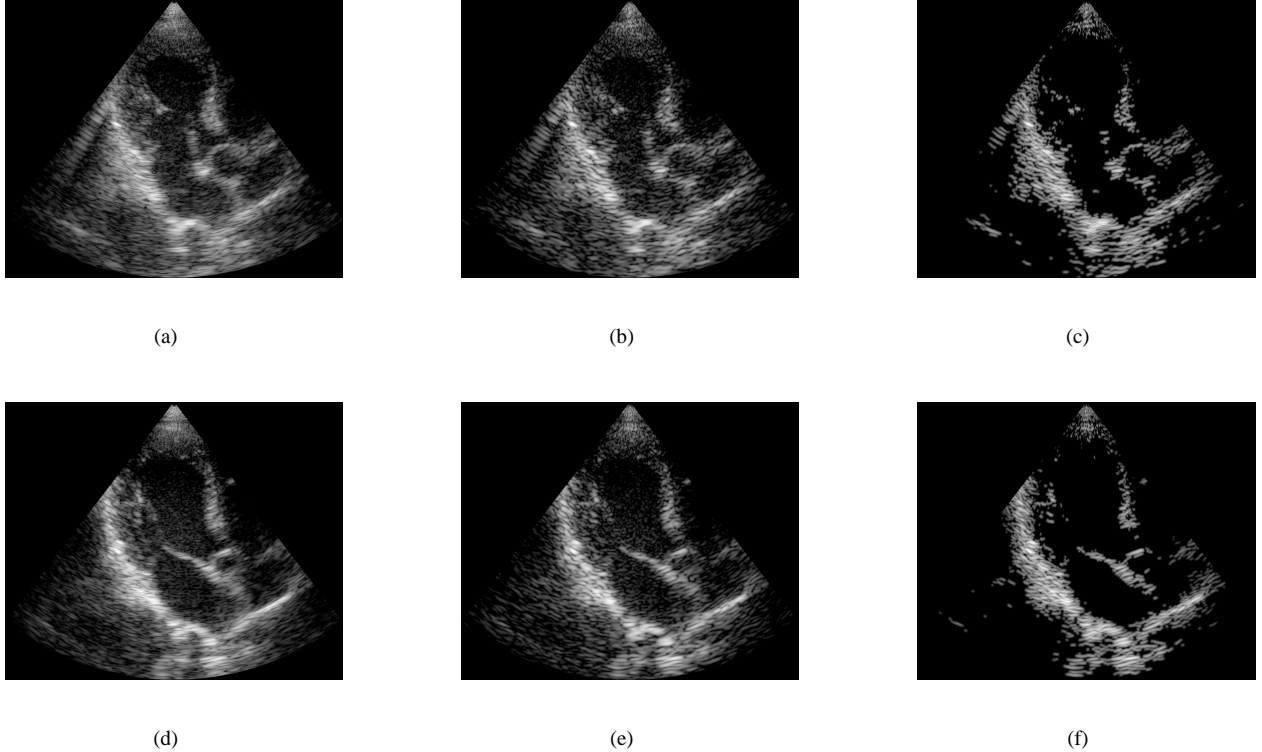


Fig. 7. Simulation results. The first row, (a)-(c), corresponds to frame 1, the second row, (d)-(f), corresponds to frame 2. (a), (d) Time domain beamforming, (b), (e) Frequency domain beamforming, l_1 optimization solution. (c),(f) Frequency domain beamforming, l_0 optimization solution.

frequency we used a subset μ of 100 DFT coefficients, which can be obtained from 120 real-valued samples by the proposed Xampling scheme. This implies 28 fold reduction in sampling and 14 fold reduction in processing rate compared to standard beamforming, which requires 3360 real-valued samples for this particular imaging setup. The difference between the sampling and processing rates stems from the complex nature of DFT coefficients. Having computed the DFT coefficients of the beamformed signal, we obtain its parametric representation by solving (22). To this end we used the NESTA algorithm [27]. This fast and accurate first-order method, based on the work of Nesterov [28], is shown to be highly suitable for solving (22), when the signal of interest is compressible with high dynamic range, which is particularly true for ultrasound imaging. An additional advantage of NESTA is that it does not depend on fine tuning of numerous controlling parameters. A single smoothing parameter, μ , needs to be selected based on a trade-off between the accuracy of the algorithm and its speed of convergence. This parameter was chosen empirically to yield optimal performance with respect to image quality.

The resulting images, corresponding to two different frames, are shown in Figs. 7 (b) and (e). Although the images are not identical to those obtained by standard beamforming (Figs. 7 (a) and (d)), it can be easily seen that l_1 optimization, based on the assumption that the signal of interest is compressible, allows to reconstruct both strong reflectors and speckle. Table II reports corresponding values of NRMSE and SSIM. Although the quantitative values are reduced compared to those obtained in Sec. IV-B, important information, e.g. the thickness of the

heart wall and the valves, as well as the speckle pattern, essential for tracking tools, are preserved.

We would like to emphasize, that the values of NRMSE and SSIM are provided in order to give a sense of performance of the proposed method. In practice, unfortunately, there are no established quantitative measures for the quality of ultrasound images. Validation is typically performed visually by sonographers, radiologists and physicians. Furthermore, our approach inherently reduces noise so that high similarity with beamforming in time may not necessarily be advantageous.

TABLE II
QUANTITATIVE VALIDATION OF BEAMFORMING IN FREQUENCY AT
SUB-NYQUIST RATE

Method	NRMSE	SSIM
Frame 1	0.0682	0.7017
Frame 2	0.0587	0.6812

To compare the proposed method with the previously developed l_0 optimization based approach, we solved (21) with OMP, while assuming $L = 25$ strong reflectors in each direction θ . Resulting images, shown in Figs. 7(c) and (f), depict the strong reflectors, observed in Fig. 7(a) and (b), while the speckle is completely lost, degrading the overall image.

B. Implementation on Stand Alone Imaging System

As a next step we implemented low-rate frequency domain beamforming on an ultrasound imaging system [29]. The lab

setup used for implementation and testing is shown in Fig. 8 and includes a state of the art GE ultrasound machine, a phantom and an ultrasound scanning probe. In our study we used a breadboard ultrasonic scanner with 64 acquisition channels. The radiated depth $r = 15.7$ cm and speed of sound $c = 1540$ m/sec yield a signal of duration $T = 2r/c \approx 204$ μ sec. The acquired signal is characterized by a narrow band-pass bandwidth of 1.77 MHz, centered at a carrier frequency $f_0 \approx 3.4$ MHz. The signals are sampled at the rate of 50 MHz and then are digitally demodulated and down-sampled to the demodulated processing rate of $f_p \approx 2.94$ MHz, resulting in 1224 real-valued samples per transducer element. Linear interpolation is then applied in order to improve beamforming resolution, leading to 2448 real valued samples. Fig. 9 presents a schematic block diagram of the transmit and receive front-end of the medical ultrasound system being used.



Fig. 8. Lab setup: Ultrasound system, probe and cardiac phantom.

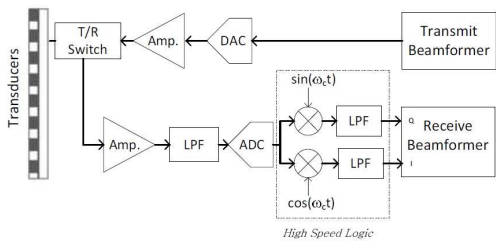


Fig. 9. Transmit and receive front-end of a medical ultrasound system.

At this point of our work, as illustrated in Fig. 10, in-phase and quadrature components of the detected signals were used to obtain the desired set of their DFT coefficients. Using this set, beamforming in frequency was performed according to (13) and (14), yielding the DFT coefficients of the beamformed signal. In this setup the sampling rate remained unchanged, but frequency domain beamforming was performed at a low rate. In our experiments we computed 100 DFT coefficients of the beamformed signal, using 120 DFT coefficients of each one of the detected signals. This corresponds to 240 real-valued samples used for beamforming in frequency. The number of samples required by demodulated processing rate is 2448. Hence, beamforming in frequency is performed at a rate corresponding to $240/2448 \approx 1/10$ of the demodulated processing

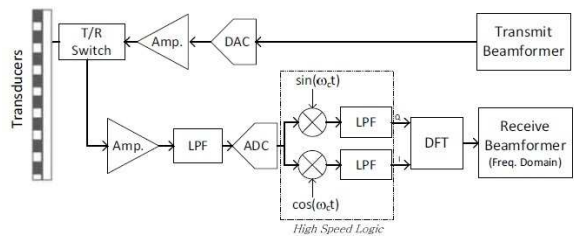


Fig. 10. Transmit and receive paths of a medical ultrasound system with beamforming in the frequency domain.

rate. Images obtained by low-rate beamforming in frequency and standard time-domain beamforming are presented in Fig. 11. As can be readily seen, we are able to retain sufficient image quality despite the significant reduction in processing rate.

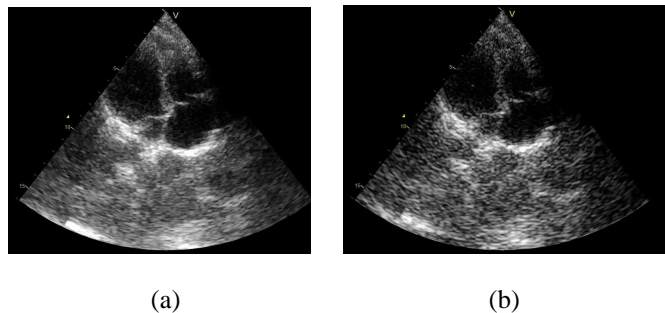


Fig. 11. Cardiac images obtained by demo system. (a) Time domain beamforming. (b) Frequency domain beamforming, obtained with 10 fold reduction in processing rate.

Our implementation was done on a state-of-the-art system, sampling each channel at a high rate. Data and processing rate reduction took place following DFT, in the frequency domain. However, by implementing the Xampling scheme described in Section IV-B, the set of 120 DFT coefficients of the detected signals, required for frequency domain beamforming, can be obtained directly from only 120 real-valued low rate samples.

VII. CONCLUSION

In this work we extended the compressed beamforming framework, proposed in [5], to a general concept of beamforming in frequency, dual to standard time domain beamforming. We have shown that when performed directly in frequency, beamforming does not require oversampling, essential for its digital implementation in time. Hence, 4-10 fold reduction in sampling rate is achieved by the translation of beamforming into the frequency domain, without compromising image quality and without involving any additional assumptions on the signal.

Further reduction in sampling rate is obtained, when only a portion of the beam's bandwidth is used. In this case the detected signals are sampled at a sub-Nyquist rate, leading to up to 28 fold reduction in sampling rate. In order to

reconstruct the beamformed signal from such partial frequency data, we rely on the fact that the beamformed signal obeys an FRI model and use CS techniques. To improve the performance of sub-Nyquist processing and avoid the loss of speckle information, we assumed that the coefficient vector is compressible. This assumption allows to capture both strong reflections, corresponding to large perturbations in the tissue, and much weaker scattered echoes, originating from microscopic changes in acoustic impedance of the tissue.

Finally, we implemented our frequency domain beamforming on a stand alone ultrasound machine. Low-rate processing is performed on the data obtained in real-time by scanning a heart with a 64 element probe. The proposed approach allows for 10 fold rate reduction with respect to the lowest processing rates that are achievable today.

Our results prove that the concept of sub-Nyquist processing is feasible for medical ultrasound, leading to the potential of considerable reduction in future ultrasound machines size, power consumption and cost.

ACKNOWLEDGMENT

The authors would like to thank GE Healthcare Haifa and in particular Dr. Arcady Kempinski for providing the imaging system and for many helpful discussions. They are grateful to Alon Eilam for his assistance with the implementation of the proposed method on an ultrasound machine.

REFERENCES

- [1] C. E. Shannon, "Communication in the presence of noise," *Proceedings of the IRE*, vol. 37, no. 1, pp. 10–21, 1949.
- [2] B. D. Steinberg, "Digital beamforming in ultrasound," *IEEE Transactions on Ultrasonics, Ferroelectrics and Frequency Control*, vol. 39, no. 6, pp. 716–721, 1992.
- [3] R. Tur, Y. C. Eldar, and Z. Friedman, "Innovation rate sampling of pulse streams with application to ultrasound imaging," *IEEE Transactions on Signal Processing*, vol. 59, no. 4, pp. 1827–1842, 2011.
- [4] M. Vetterli, P. Marziliano, and T. Blu, "Sampling signals with finite rate of innovation," *IEEE Transactions on Signal Processing*, vol. 50, no. 6, pp. 1417–1428, 2002.
- [5] N. Wagner, Y. C. Eldar, and Z. Friedman, "Compressed beamforming in ultrasound imaging," *IEEE Transactions on Signal Processing*, vol. 60, no. 9, pp. 4643–4657, 2012.
- [6] Y. C. Eldar and G. Kutyniok, "Compressed sensing: Theory and applications," *New York: Cambridge Univ. Press*, vol. 20, p. 12, 2012.
- [7] T. Michaeli and Y. C. Eldar, "Xampling at the rate of innovation," *IEEE Transactions on Signal Processing*, no. 99, pp. 1121–1133, 2011.
- [8] M. Mishali, Y. C. Eldar, and A. J. Elron, "Xampling: Signal acquisition and processing in union of subspaces," *IEEE Transactions on Signal Processing*, vol. 59, no. 10, pp. 4719–4734, 2011.
- [9] M. Mishali, Y. C. Eldar, O. Dounaevsky, and E. Shoshan, "Xampling: Analog to digital at sub-Nyquist rates," *IET circuits, devices & systems*, vol. 5, no. 1, pp. 8–20, 2011.
- [10] K. Gedalyahu, R. Tur, and Y. C. Eldar, "Multichannel sampling of pulse streams at the rate of innovation," *IEEE Transactions on Signal Processing*, vol. 59, no. 4, pp. 1491–1504, 2011.
- [11] E. Baransky, G. Itzhak, I. Shmuel, N. Wagner, E. Shoshan, and Y. C. Eldar, "A Sub-Nyquist Radar Prototype: Hardware and Algorithms," *submitted to IEEE Transactions on Aerospace and Electronic Systems, special issue on Compressed Sensing for Radar*, Aug. 2012.
- [12] H. L. Van Trees, *Detection, Estimation, and Modulation Theory, Optimum Array Processing*. Wiley-Interscience, 2004.
- [13] J. A. Jensen, "Linear description of ultrasound imaging systems," *Notes for the International Summer School on Advanced Ultrasound Imaging, Technical University of Denmark July*, vol. 5, 1999.
- [14] M. O'Donnell, W. E. Engeler, J. T. Pedicone, A. M. Itani, S. E. Noujaim, R. J. Dunki-Jacobs, W. M. Leue, C. L. Chalek, L. S. Smith, J. E. Piel, R. L. Harris, K. B. Welles, and W. L. Hinrichs, "Real-time phased array imaging using digital beam forming and autonomous channel control," in *Ultrasonics Symposium, 1990. Proceedings., IEEE 1990*. IEEE, 1990, pp. 1499–1502.
- [15] A. V. Oppenheim, R. W. Schaffer, J. R. Buck *et al.*, *Discrete-time signal processing*. Prentice hall Upper Saddle River, 1999, vol. 5.
- [16] Z. Wang, A. C. Bovik, H. R. Sheikh, and E. P. Simoncelli, "Image quality assessment: From error visibility to structural similarity," *IEEE Transactions on Image Processing*, vol. 13, no. 4, pp. 600–612, 2004.
- [17] T. Sarkar and O. Pereira, "Using the matrix pencil method to estimate the parameters of a sum of complex exponentials," *IEEE Antennas and Propagation Magazine*, vol. 37, no. 1, pp. 48–55, 1995.
- [18] P. Stoica and R. Moses, *Introduction to spectral analysis*. Prentice Hall Upper Saddle River, NJ, 1997, vol. 89.
- [19] M. Rudelson and R. Vershynin, "On sparse reconstruction from fourier and gaussian measurements," *Communications on Pure and Applied Mathematics*, vol. 61, no. 8, pp. 1025–1045, 2008.
- [20] J. A. Tropp and A. C. Gilbert, "Signal recovery from random measurements via orthogonal matching pursuit," *IEEE Transactions on Information Theory*, vol. 53, no. 12, pp. 4655–4666, 2007.
- [21] Y. Notomi, P. Lysyansky, R. M. Setser, T. Shiota, Z. B. Popovic, M. G. Martin-Miklovic, J. A. Weaver, S. J. Oryszak, N. L. Greenberg, R. D. White, and J. D. Thomas, "Measurement of ventricular torsion by two-dimensional ultrasound speckle tracking imaging," *Journal of the American College of Cardiology*, vol. 45, no. 12, pp. 2034–2041, 2005.
- [22] M. S. Suffoletto, K. Dohi, M. Cannesson, S. Saba, and J. Gorcsan, "Novel speckle-tracking radial strain from routine black-and-white echocardiographic images to quantify dyssynchrony and predict response to cardiac resynchronization therapy," *Circulation*, vol. 113, no. 7, pp. 960–968, 2006.
- [23] E. Candès and J. Romberg, "l1-magic," *www.l1-magic.org*, 2007.
- [24] M. Grant, S. Boyd, and Y. Ye, "CVX: Matlab software for disciplined convex programming," 2008.
- [25] A. Beck and M. Teboulle, "A fast iterative shrinkage-thresholding algorithm for linear inverse problems," *SIAM Journal on Imaging Sciences*, vol. 2, no. 1, pp. 183–202, 2009.
- [26] E. T. Hale, W. Yin, and Y. Zhang, "A fixed-point continuation method for l1-regularized minimization with applications to compressed sensing," *CAAM TR07-07, Rice University*, 2007.
- [27] S. Becker, J. Bobin, and E. J. Candès, "NESTA: a fast and accurate first-order method for sparse recovery," *SIAM Journal on Imaging Sciences*, vol. 4, no. 1, pp. 1–39, 2011.
- [28] Y. Nesterov, "Smooth minimization of non-smooth functions," *Mathematical Programming*, vol. 103, no. 1, pp. 127–152, 2005.
- [29] A. Eilam, T. Chernyakova, Y. C. Eldar, and A. Kempinski, "Sub-nyquist medical ultrasound imaging: En route to cloud processing," *submitted to GlobalSIP 2013*.